OPTICAL MEASUREMENTS FOR ATTITUDE CONTROL AND SHAPE RECONSTRUCTION AT THE ROSETTA FLYBY OF ASTEROID LUTETIA

Mathias Lauer[(1)], Sabine Kielbassa[(2)], Ramon Pardo[(3)]

[(1)]ESA/ESOC
[(2)]Telespazio VEGA Deutschland GmbH located at ESOC
[(3)]GMV located at ESOC

Robert-Bosch-Strasse 5, 64293 Darmstadt, Germany
+49 6151 900, <firstname>.<lastname>@esa.int

***Abstract**: The ESA interplanetary spacecraft (S/C) Rosetta was launched in March 2004 to rendezvous with comet Churyumov-Gerasimenko in 2014. In July 2010 the S/C flew by asteroid Lutetia. Optical measurements taken by on-board CCD cameras were used to navigate the S/C towards the requested flyby conditions and to control autonomously the attitude of the S/C during the flyby phase proper in order to ensure that payload instruments were pointing towards the asteroid. In preparation of the flyby, extensive tests were carried out to characterise the tracking performance of the navigation camera for the variety of observing conditions over the flyby period. Based on these tests, the operational settings for the camera were selected to ensure that the asteroid was accurately tracked. After the flyby, a series of images taken by the on-board science camera was analysed to reconstruct the flyby geometry and to generate a coarse shape model. The geometry reconstruction was based on the identification of landmarks on the asteroid. The shape model was derived using a combination of silhouette and shadow carving methods.*

***Keywords:** Optical Navigation, Asteroid Flyby, Autonomous Tracking, Shape Reconstruction*

1. Introduction

The ESA interplanetary spacecraft (S/C) Rosetta was launched in March 2004 to rendezvous with comet Churyumov-Gerasimenko in 2014. The overall trajectory contains four planetary swing-bys, three at the Earth and one at Mars. The scientific outcome of the mission is enhanced by two asteroid flybys, one in September 2008 at asteroid Steins, and the second in July 2010 at asteroid Lutetia, after the last Earth swing-by.

For the asteroid flybys, optical measurements taken by on-board CCD cameras were used to navigate the S/C towards the requested flyby conditions and to control autonomously the attitude of the S/C during the flyby phase proper in order to ensure that payload instruments were pointing towards the asteroid. The Steins flyby was conducted successfully, however with degraded performance in the autonomous pointing. An overview of the overall optical data processing, including performance analyses for the various phases of the Steins flyby navigation, was already presented at the ISSFD in 2009 (see [1]). For the Lutetia flyby, a similar approach

for the optical data processing was followed, with two new major aspects that are presented in this paper in dedicated sections:

- To improve the camera tracking performance for the Lutetia flyby, a sequence of tests were carried out to tune the main parameters of the camera software. A configuration was established and commanded to the camera prior to the flyby. This configuration led to a successful and accurate tracking of the asteroid over the flyby.
- In preparation of the near comet operations, software has been developed at ESOC to navigate around a small body based on optical data. This software includes programs to identify landmarks in images of the body, to reconstruct the positions of the landmarks and of the camera relative to the body, and to generate a coarse shape model. These methods were also applied to post-process the Lutetia images that were taken by the on-board science camera during the flyby.

1. Autonomous Asteroid Tracking

The degraded pointing performance during the Steins flyby was mainly caused by the presence of warm pixels (i.e. pixels with increased dark current) in combination with size and brightness of the target and specific features of the navigation camera software (see [1] for details). To improve the pointing accuracy for Lutetia, a different configuration of the on-board camera during autonomous tracking had to be selected. The main parameters to be tuned were the integration time and the detection threshold. This threshold determines the minimum signal in a pixel that is required such that it is considered as part of the extended object.

2.1 Warm Pixel Characterisation

As a first step in the tuning process, the warm pixels of the cameras (nominal and redundant) were characterised. For the detection of warm pixels, full images during slews were acquired with 2 s integration time and analysed. As the camera did not have an opaque cover, it was not possible to acquire dark images. By acquiring the images during a slew, it was possible to distinguish warm pixels from bright star images. Faint stars were anyway not visible due to the attenuation filter that was selected for the images. In this way, a list of warm pixels (position on CCD and signal rate) was established for both navigation cameras. As an example, fig. 1 shows the list of the 32 pixels with the highest signal rate for three selected series of images. Fig. 1 also shows the dependency of the signal rate on the CCD temperature of the sensor. Some of the worst pixels were located outside the expected positions of the tracking window during Lutetia approach, such that they could be discarded for the tuning of the camera settings. Based on a S/C thermal characterisation, the camera sensor temperature expected for the Lutetia flyby was known in advance. This allowed to establish a lower bound on the detection threshold for the asteroid tracking as function of integration time. The list of warm pixels was monitored over several weeks prior to the flyby. It turned out, that the number and signal rate of the warm pixels was quite stable.

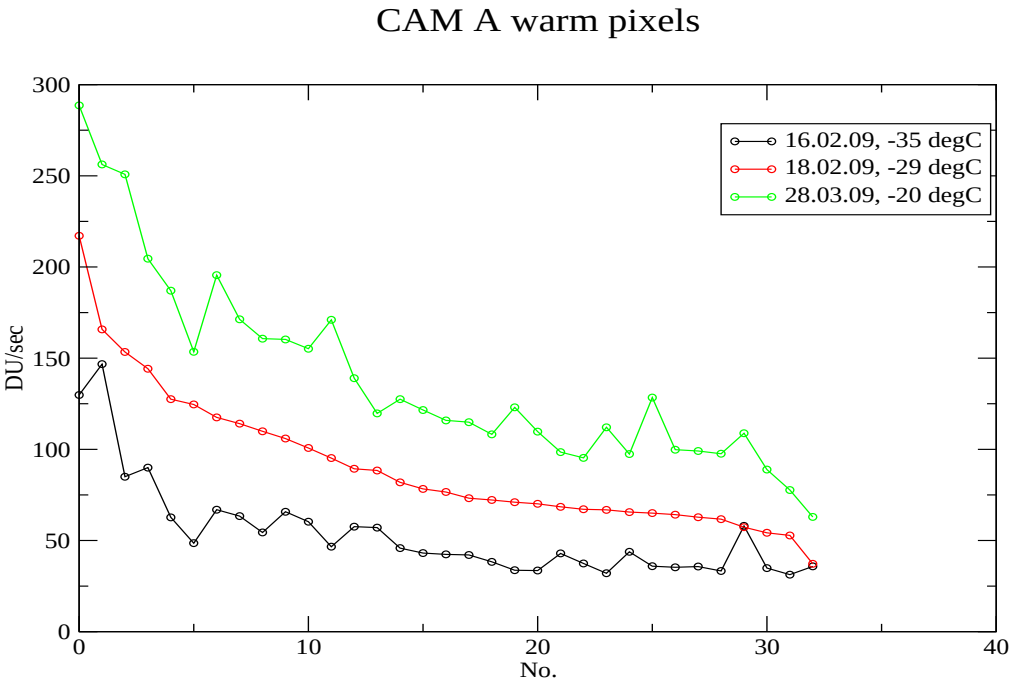

Figure 1. Camera warm pixel list

2.2 Star Tracking Test

At far approach, the apparent brightness of Lutetia was predicted to be of ca. -0.6 instrumental magnitude. To verify the camera performance, two stars were tracked with a number of parameter combinations for detection threshold and integration time. The selected stars were Vega and Spica, which are slightly fainter than Lutetia.

In addition, the S/C was commanded to follow an attitude such that the path of the star on the CCD of the camera was describing a circle. As a result, the star centre position relative to the grid of pixels was changing during the tracking test. For the tuning of the detection threshold, the maximum signal in any of the pixels corresponding to the star is important. It was expected that this number would depend on the relative position, due to the variation of the point spread function. In fact, it turned out that also the total signal rate (sum of the signals over the full matrix of the point spread function) showed a considerable dependency on the relative target centre position. Based on the acquired data, it was concluded that for the ratio between the maximum signal in a pixel of the object matrix and the maximum total signal of the object matrix observed for any relative position, a range from 15% to 75% should be assumed. I.e. in the worst case, only 15% of the target signal would be detected by the brightest pixel belonging to the object. Correspondingly, the number of pixels detected by the camera was varying between 1 and 4.

The accuracy of the tracking was usually better than one pixel, but occasionally disturbed by singe event upsets (SEU) caused by cosmic particles. The number of SEU occurrences was, as expected, proportional to the size of the tracking window. For a 250 by 250 pixel size window,

about 2% to 5% of the frames was disturbed by an SEU, whereas for a 500 by 500 pixel size window already ca. 10% to 20% of the frames was disturbed. The effect of the SEU on the position measured by the camera also depended on the size of the window, as the target position is computed by the camera as an average position of all detected pixels. For the Lutetia approach phase, with a target size of only a few pixels, it was concluded, that this disturbance could be reduced by the selection of a smaller window size, and the remaining disturbance could be filtered out by the on-board AOCS target direction estimation algorithm that was processing the raw image measurements.

2.3 Integration time and detection threshold

The tuning of the integration time was based on the maximum surface brightness of the asteroid which would occur at zero degree phase angle. It was set to 0.34s, which would lead to a filling ca. 75% of the capacity in the brightest pixels.

The detection threshold had to be sufficiently high in order to avoid tracking of a warm pixel, but at the same time to be sufficiently low to ensure tracking of the asteroid. A lower bound could be derived from the warm pixel characterisation, and an upper bound from the star tracking test. A preliminary threshold of 100 DU's was derived as an optimum value.

2.4 Extended target tracking tests

To validate the tuning of the camera also for extended objects, the occasion of the last Earth swing-by was used to track the Moon and the Earth. It is clear that it was not possible to operate the camera with exactly the same settings as for the Lutetia flyby, due to the different apparent brightness of the targets. The integration time was therefore scaled down for the test cases. One test was conducted after the swing-by on 30 November 2009. On this day, the Moon and the Earth had an apparent size of 3 and 11 pixels respectively. These sizes correspond to the size of Lutetia at ca. closest approach (CA) – 8 hours and CA – 2 hours. Another test was conducted prior to the swing-by on 13 November 2009 with the Earth, which had an apparent diameter of 670 pixels. This was the maximum size that was expected to occur for the Lutetia flyby. In all cases, the tracking was proven to be successful, i.e. stable and with reasonable accuracy (e.g. less than 1 pixel for object sizes of 3 and 11 pixels, and less than 15 pixels for an object size of 670 pixels).

2.5 Lutetia tracking

Based on the warm pixel characterisation, the results of the tracking tests with stars (Vega and Spica), Earth and Moon, a preliminary setting for the Lutetia flyby was selected (0.34s integration time, 100 DU's detection threshold). The validity of this setting was continuously checked during the Lutetia approach phase starting with first detection up to the final GO/NOGO decision for the autonomous tracking only a few hours prior to the flyby. Images taken during

navigation slots were analysed for warm pixels and for the prediction of the expected target brightness. After the first commanding of the camera into tracking mode, several target parameters in telemetry (e.g. position, size, signal, envelope) were continuously monitored.

It turned out that the preliminary setting was also valid for the actual flyby and did not require any update. The asteroid was tracked with sufficient accuracy to allow to acquire high resolution images with the science narrow angle camera.

2. Landmarks and Shape

3.1. Landmark Determination

In preparation for the near comet operations of Rosetta, a series of software tools has been developed to process optical data for navigation. The basic measurement type in this context is the direction from the camera to a landmark on the object. Reconstruction of S/C position and body attitude can then be achieved based on suitable estimation algorithms. For the detection and measurement of landmarks in images, several schemes have been presented in the literature (see e.g. [2] and references therein). Due to the uncertainty in the optical appearance of the comet nucleus and the requirement for flying close orbits very soon after arrival, a robust technique was selected as baseline where landmarks are determined and matched using a graphical user interface (GUI). Pairs of images are shown side by side in an area of the GUI (see fig. 2 and [3]). By visual inspection, the operator selects with the mouse a pixel in each image which represents the same landmark. A series of images is processed in this way, and the result is a list of landmark observations, each of which consists of an image identifier, a landmark identifier and the pixel position of the landmark in the image. In addition, the operator assigns already an uncertainty to the measurement in pixels. Based on the optical properties of the camera, the pixel positions are subsequently converted into directions in camera frame.

This s/w tool for landmark detection has been applied to a series of Lutetia images that were acquired by the Osiris science narrow angle camera during the flyby. Due to the high flyby speed of the S/C of ca. 15 km/s, the apparent size of the asteroid was changing considerably between the images. In the first of the processed images, taken about 50 minutes prior to closest approach, the apparent diameter of the body was less than 150 pixels. Whereas at CA, the apparent diameter was even exceeding the full frame of 2048 by 2048 pixels. In total, 1788 landmark observations were recorded, with a total of 89 different landmarks in 42 images.

In a first step, S/C and landmark positions were reconstructed from the optical measurements using a bundle adjustment technique. A detailed description of this process has been provided in [3]. This initial reconstruction was not using any kinematic model, but only fitting the geometric positions of the landmark and the camera to the observations in an arbitrary scaled frame.

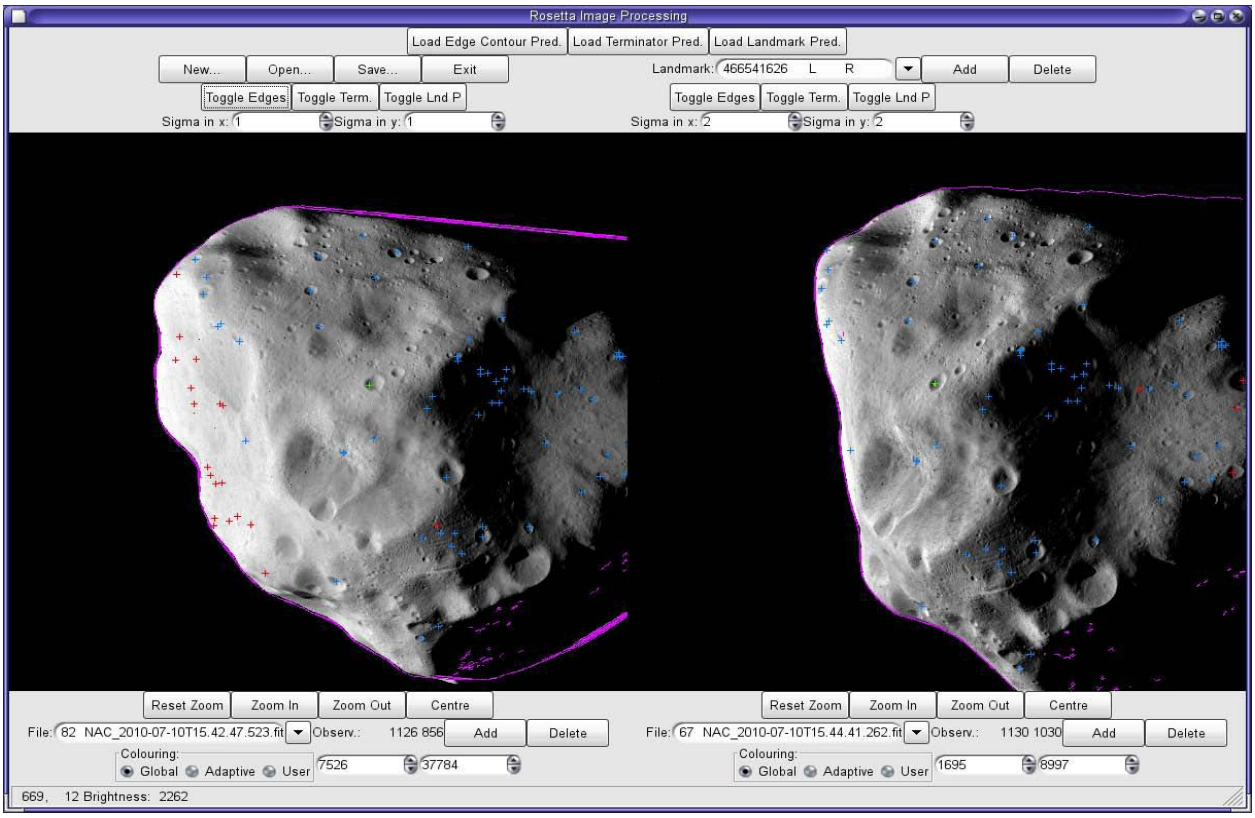

Figure 2. GUI for landmark determination

In a second step, a refinement of the reconstruction was achieved by using a kinematic model. A linear motion of the centre of the asteroid relative to the S/C has been assumed with unknown parameters for the initial position and the initial velocity. For the landmarks, it was assumed that they are located at a fixed position in a frame that is rotating around a fixed axis with a constant angular rate. The direction of the rotation axis and the angular rate were also treated as unknown parameters. The model equation for a landmark observation was therefore as follows:

$$n_{ij} = < S(\eta_i) C_i (p_0 + v_0 t_i + A^t L_j) > \qquad (1)$$

where

- n_{ij} is the direction from the camera to the landmark number j in image number i in camera frame,
- p_0 and v_0 denote the initial position and velocity of the asteroid relative to the S/C in inertial frame at an initial epoch (latest estimate of the time of CA),
- t_i is the acquisition time of image i relative to the initial epoch,
- L_j is the position of landmark j in the asteroid fixed frame,
- C_i is the nominal attitude of the camera at acquisition of image i and

- $S(\eta_i)$ is a small rotation from nominal to actual camera frame for image i to account for misalignments and attitude control errors.

The square bracket indicates normalisation of the vector within the brackets to a unit vector.

The rotation matrix of the asteroid is broken down into three components:

$$A = R_z(\varphi_i)S(\varepsilon)A_0 \qquad (2)$$

where

- $R_z(\varphi_i)$ is a rotation around the z-axis by the phase angle $\varphi_i = \varphi_0 + \omega t_i$ at acquisition time of image I,
- φ_0 is the initial phase of the asteroid frame,
- ω is the rotation rate of the asteroid,
- A_0 is the nominal attitude of the asteroid at the initial epoch, and
- $S(\varepsilon)$ is a small rotation of the initial asteroid frame to account for errors in the nominal initial asteroid attitude.

For the validity of this model, several assumptions needed to be verified:

- The relative motion of the S/C is in fact not linear, but is subject to gravity (Sun and asteroid) and to disturbances (solar radiation pressure). For the time period of the observations however, the deviation of the relative orbit from the linear one is below the detection limit of the camera, i.e. below a tenth of a pixel.

- Due to the high flyby speed, the apparent direction of the landmark as seen by the camera is distorted by aberration (light time correction plus stellar aberration). This shift is not negligible (up to 3 pixels). However, the differential aberration (i.e. variation of aberration within the same image) is again below the camera detection limit. The accuracy of the nominal camera attitude was assumed to be 10 mdeg (1 σ) around each axis. The effect of the aberration could therefore be absorbed in the estimation process by the corrections to the camera attitude for each image.

- The attitude motion of the asteroid was not necessarily a pure rotation around a fixed axis. But also in this case, any deviations from this pure rotation would not be observable from the landmark observations during this short period of time (see discussion of results below).

The reconstruction consisted in estimating all unknown parameters from the landmark observations. These parameters were the initial relative position and velocity of the S/C (6 parameters), the landmark positions in asteroid frame (3 parameters per landmark), correction angles for the camera attitude (3 parameters per image), the initial phase and rotation rate of the asteroid (2 parameters) and the correction angles for the initial asteroid attitude (3 parameters). The reconstruction was achieved by an iterative process. In each step, the measurement equations were linearised around a reference parameter vector and the solution found from the minimum variance estimator. The solution was used as reference parameter vector for the next iteration step.

For a meaningful solution, including error estimates, the a-priori knowledge of the parameter vector with uncertainties had to be determined:

- For the initial S/C relative position and velocity the estimate of the state vector at CA from the nominal orbit determination process was taken (see also [4]). This estimate was based on radiometric data from S/C tracking and optical data. The optical data included ground based observations of the asteroid, on-board observations until 12 hours prior to the flyby and direction measurements by the navigation camera recorded during the autonomous tracking phase. For the position uncertainties, conservative estimates were taken. The flyby was roughly aligned with the –x axis of the inertial frame. For the uncertainty along the x direction, the uncertainty of the flyby time as estimated one day prior to CA was converted into a position uncertainty. For the perpendicular axes, a 3 σ error of 20 km was taken. This decision was based on the fact, that the reconstructed flyby position in the B-plane was ca. 20 km away from the last prediction prior to the flyby. Based on independent orbit determinations of the S/C and the asteroid the uncertainty in the flyby velocity was set to 1 cm/s per axis 1 σ (see [5]).

- For the initial position of the landmarks, the positions as estimated in the first step (bundle adjustment) were used (see [3]. They were however scaled and rotated to align them as far as possible with a shape model that was provided by the Osiris team (see [11]). This was done to allow a better comparison with the external data. The uncertainties were set to 10 km 1 σ in each direction. This was considered sufficiently large in order not to constrain the solution too much.

- For the uncertainty in the camera attitudes, a value of 10 mdeg around each axis has been considered. This accounts for a residual misalignment, but also for the fact that the performance of the attitude estimator was worse under the flyby conditions compared to stable pointing conditions. In addition, the star tracker boresight is perpendicular to the boresight of the science camera, such that the largest error of the star tracker attitude estimate which occurs around its boresight is translated into a depointing of the camera boresight.

- The remaining parameters are related to the attitude of Lutetia. According to [6], the rotation axis was estimated to be within 5° of (α = 52°, δ = 12°) in equatorial coordinates based on ground observations. The rotation period was given as 8.168270 +/- 0.000001 hours in [6]. These data were taken as initial estimates and uncertainties for the rotation axis and rotation rate for the reconstruction process.

With these initial parameters and their uncertainties, the estimation process converged quickly within less than 10 iterations. In the last step, the positions of the camera and the landmarks in the solution vector were changing by less than 1 m.

The initial position of the asteroid relative to the S/C was shifted by ca. 18 km along the flyby direction compared to the a-priori estimate. The initial relative velocity in the final solution differed from the initial guess by less than 1 mm/s in each component. This difference is insignificant, as the formal uncertainty in this parameter did not improve compared to the initial uncertainty of 1 cm/s.

The small corrections to the nominal camera attitudes were all well below the 3σ value of the initial uncertainty. They were typically in the range from 3 to 11 mdeg around the perpendicular axes of the image plane, in absolute values. As an independent verification of the attitude, the measured position of Saturn in two images was compared against the prediction. As the S/C was slewing to follow the asteroid with the payload boresight, the planet was crossing the field of view of the science camera for about 15 minutes. During this period of time, several images were acquired, however not with full frames of 2048 by 2048 pixels. In addition, landmarks were not identified in all images taken during the flyby. However, there were two images in this period,

where the planet appeared in the acquired subwindow, and where the attitude was corrected by the overall estimation process. The difference in the position (measured minus predicted) was (-2,-1) pixels in the first image, and (-3,0) pixels in the second (where no attempt has been made to determine the centre position of Saturn to sub-pixel accuracy). This has to be compared with the uncertainty in the reconstruction which was +/-(1.5,1.7) pixels 1σ for the first image and +/-(1.2,1.3) pixels 1σ for the second.

The difference in the rotation rate of the asteroid between initial and final solution was also insignificant, because it was orders of magnitude lower than the formal uncertainty. In order to check, whether the solution was too much constraint by the initial estimate and uncertainty of the rotation rate, another run was performed were the uncertainty in the initial estimate was increased to 1°/hr. The estimated value for the rotation rate became 0.37°/hr higher than the initial value, but with an uncertainty of 0.16°/hr (1σ). The results in other parameters did not change considerably w.r.t. to the reference solution. Also the characteristics of the residuals in the landmark measurements hardly changed. It was concluded that the estimate of the rotation rate based on ground observations was consistent with the landmark measurements, and that these measurements did not contain enough information to improve this estimate, which was therefore retained as initial estimate together with its small uncertainty in the reference solution.

The direction of the asteroid spin axis was shifted slightly compared to the initial estimate from literature [6], but the formal uncertainty significantly reduced. The final solution was: 52.9° +/- 0.4° (1σ) in right ascension and 12.4° +/- 0.3° (1σ) in declination. The result derived after the flyby by the Osiris science team was 51.8° +/- 0.4° in right ascension, and 10.8° +/- 0.4° in declination (see [7]). These results agree within the specified uncertainties, although only marginally for the value of the declination if the uncertainties in [7] are already 3σ values.

The landmark positions were estimated with uncertainties of about 1 km. But these values rather reflect the uncertainty of the rotation axis relative to the set of landmarks, and of the origin of the asteroid frame relative to the S/C flyby orbit. A better way to indicate the accuracy of the landmark positions relative to each other is the covariance of the expected position of a landmark, given the position of all other landmarks. This was computed for each landmark based on the full covariance matrix of the estimation process. With the exception of two landmarks, that have not been observed frequently, the mean relative position uncertainty was 31 m, 43 m and 77 m, along the three body axes. This has to be compared with the equivalent pixel resolutions of the images which were in the range from 55 m at CA up to 786 m for the first image at approach.

In addition, reconstructed landmark positions were compared to shape models from the Osiris science team and from a team at the DLR Institut für Planetenforschung. Based on four landmark measurements in an image near CA, the corresponding positions within the shape models were reported to ESOC by both teams (see [8] and [9]). The measurements were only accurate to integer pixels, such that an agreement better than the equivalent pixel resolution could not be expected. The coordinate systems in which the landmark positions were provided were not aligned, and even not consistently scaled. By comparing distances between the landmarks, the distances were in the mean 0.9% larger in [8], and 0.7% larger in [9]. The misalignments between the axes perpendicular to the rotation axis were -0.8° and -1.4° in [8], and 0.0° and 0.8° in [9]. If the scaling and the misalignment was removed, the differences in any of the position components compared to [8] was between -69 m and +71 m, and compared to [9] between -131 m and 171 m. The origins of the coordinate systems in [8] and [9] were shifted (after rescaling

and removal of misalignment) along the z-axis of the asteroid frame by 0.2 km and 2.4 km respectively.

Based on the estimation result, the position of any landmark, or any other point tied to the system of landmarks relative to the S/C could be computed at any time from the model equations (using the formula in brackets of eqn (1) above). Also the time of closest approach to any of those points can be derived. However, this is still not sufficient to determine the time of CA w.r.t to the centre of mass of the asteroid, because its position on the rotation axis of the asteroid frame is not known. The determined positions of the measured landmarks were almost centred around the rotation axis, and were spread between 1.7 km and 45 km along the rotation axis. Based on an assumed radius of 50 km, the centre of mass would be not far away from the centre of the coordinate system. For this centre position, the time of closest approach is 15:44:53.556 UTC on July 7 at a flyby distance of 3164.742 km. For each positive shift of 1 km along the rotation axis, the flyby time decreases by 38 ms.

3.2. Shape Reconstruction

After reconstruction of the flyby geometry, a coarse shape model was determined from the images. The selected method was silhouette and shadow carving (see e.g. [10]).

In a first step, the images were pre-processed. Small clusters of bright pixels, not belonging to the asteroid (mainly single event upsets and Saturn) were removed to avoid interference with the silhouette carving of the asteroid. Also, the effect of the camera distortion was corrected, such that a straight line in space is projected onto a straight line in the image.

3.2.1 Silhouette Carving Method

In the process of reconstructing asteroid Lutetia's shape, the first phase was the silhouette carving.

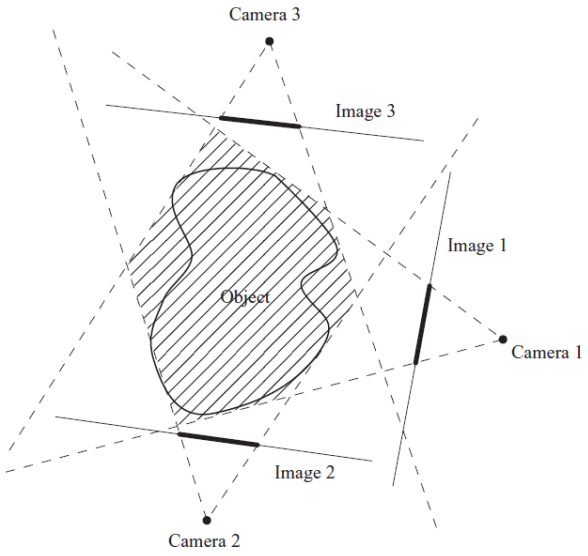

Figure 3. Silhouette Carving Method (from [10])

Through this method, a volume bigger than the one of the body is considered and images are processed sequentially to carve out the parts that fall out of the body silhouette. The result is the visual hull of the body that is a conservative estimation of the volume. In this sense, it is guaranteed that the body is contained in the visual hull but not all extra volume has been carved out. This method is fast, robust, easy to implement and silhouette-consistent.

The illumination's limit (terminator) implies that the complete silhouette of the figure of the body can not be fully seen in an image since one side will normally fall on the dark side of the body. Therefore, it is not possible to carve out on regions within the shadow casted by the body itself.

Figure 4. Simulated image (left), processed shadow (centre), area of empty space in red (right)

From the flyby geometry it was possible to derive the camera position, the camera attitude and the Sun direction in Lutetia's frame. The images were processed in order to classify every pixel within three categories: lit, candidate and empty:

- Pixels brighter than a certain threshold were defined as lit.
- Those pixels that were on the casted shadow path were flagged as candidates. To ensure that a non-lit pixel was a candidate pixel, the Sun direction was followed from the pixel under evaluation until a lit pixel was found on the way.
- The rest of the pixels were classified as empty. Only the parts of the initial volume falling on empty pixels were carved out.

The shape of asteroid Lutetia has been initialised with a cuboid (140km x 140km x 140km) containing the true shape. The volume of the cuboid was then discretized in 3D into smaller cubes (1km x 1km x 1km). Each cube was mapped to a pixel on every image by using the flyby geometry. The cubes falling in at least one image on an empty pixel were removed.

3.2.2 Shadow Carving Method

In a second phase, the shadow carving was used. This method resolves lit-shadow contradictions between the model coming from the silhouette carving and the images.

To achieve this, checking if a non-lit pixel on an image would be non-lit on the current shape model is needed. If it is not the case, all cubes outside the path of the shadow can be removed. Similarly, a cube that is lit on an image has to be lit on the shape model and no other cube can be ahead on the Sun direction. Any cube on the way can be removed. Following this rule, the shape becomes photo-consistent in a binary way: lit or non-lit.

Figure 5. Shadow carving method (from [10])

The silhouette carving alone cannot carve within concave regions; however, once a good visual hull is obtained, the shadow carving method can help characterise local depressions such as valleys or craters if enough Sun-asteroid-spacecraft configurations are given.

Due to the limited number of images and restricted viewing conditions, the resulting model is actually bigger than the asteroid and reflects the real shape only at specific locations, e.g. which appear as part of the limb in one of the images. However, for those regions the method provides accurate results.

The reconstruction of the asteroid shape was performed with a prototype software that was developed for the comet phase where optical navigation relative to landmarks will be used operationally.

3.2.3 Implementation Aspects

Storage strategy

Each cube is represented by its coordinates (i, j, k) within the cuboid system. Therefore, storing the information of a 3D discretized volume requires memory space of the order n^3, being n the number of small cubes per spatial axis. This is problematic in terms of computational memory and it increases very quickly when going to higher resolution. Instead, the storage can be reduced to a memory space of the order n^2 by storing cube segments (i, j, k_i, k_f), being k_i and k_f first and last connected cubes. Several segments can be assigned to the same (i, j) coordinates. In this sense the information stored is related to the surface and not to the interior of the shape.

Other storage strategies, such as octrees, are more efficient but would require higher implementation effort.

Multi-scale approach

Several algorithms can reduce the computational time at the carving stage. One of them was to check segments against the silhouette instead of individual cubes. The segments are cut or divided if required.

The other one is to start with a low number of cubes which reduces computation time. Subsequently, this shape is used as a starting shape and the number of cubes is increased by a factor of two in all three dimensions. This increases the number of cubes by eight but the number of segments only by four. Since the accuracy of the method is related to the cube size, a full layer of new cubes has to be added on the outside of the previous shape. When re-running the method the amount of cubes to be checked is only of order n^2 instead of n^3.

Surface reconstruction

The surface is derived by checking if a given cube has all its neighbours. If a neighbour is missing then the corresponding façade of the cube is part of the body surface. Each façade is then divided into two triangles. The relation and numbering between façades and vertices has to be carefully accounted for.

The resulting surface has sharp edges that are aligned with the coordinate axes. A surface smoothing algorithm is used to approximate the surface normals with higher accuracy. It is an algorithm that can be used recursively up to the approximation level required. Each vertex is connected with n other vertices in orthogonal directions being n from three to six. Each new vertex position is computed as:

$$\left(\vec{\mathrm{v}}\right)^{new} = \frac{\vec{\mathrm{v}} + \sum_{i=1}^{n} \vec{\mathrm{v}}_i}{n+1} \qquad (2)$$

3.2.4 Lutetia Results

The derived shape model has been compared with the images by projecting the expected contours. Examples are shown in fig. 2 as purple lines. The agreement is very good at the limb. As soon as the terminator is crossed, the contour does not follow anymore the edge of the body, as it is not possible to distinguish between empty space and shadow.

As another validity check, the distance of the reconstructed landmark positions to the shape model has been computed. The results are shown in fig. 6. Negative distances indicate, that the landmark is below the shape model. As expected, this applies for almost all landmarks. Only a small number of landmarks are outside the model, but by less than a semi-diagonal of a cube in the cuboid system. A considerable number of landmarks are less than one km away from the shape model. But there are also many landmarks which are located far inside the reconstructed shape. This is due to the limitations of the carving method, e.g. when landmarks are located in the big depression on the asteroid surface that could not be carved out.

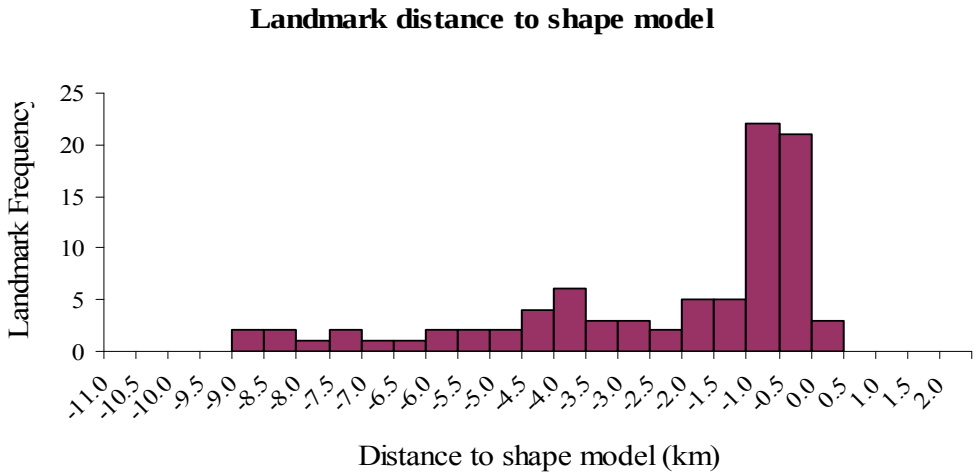

Figure 6. Comparison of shape with landmark positions

4. Summary and conclusion

The autonomous tracking of Lutetia over the flyby was overall successful and the achieved pointing performance within the specification of the S/C design. The science camera could acquire high resolution images of the asteroid as planned. This was possible due to an extensive preparation campaign, where sequences of tracking tests with the navigation camera with a considerable number of parameter combinations were run before the flyby. A variety of targets (stars, Moon and Earth) were chosen which were as far as possible representative of the appearance of the asteroid during the flyby, including the phase several hours before closest approach when the asteroid was still a point like light source. As a result of the tests, a setting of the camera parameters (e.g. integration time and detection threshold) was derived that was finally applicable for the complete flyby.

The Lutetia flyby has also been used for testing software components that were developed for the comet phase of the Rosetta mission:

1788 landmark observations were generated from images of the science camera acquired during a period of roughly one hour around closest approach. The landmark positions in the images were created with a graphical user interface by an operator. For the validation of the measurements, the observations were fitted to a kinematic model which allowed to determine the position of the landmarks in asteroid frame to a relative accuracy of ca. 50 m, which corresponds to the equivalent pixel size at closest flyby distance, and to ca. $1/1000^{th}$ of the body radius.

After reconstruction of the flyby geometry, a combination of silhouette and shadow carving methods has been applied to compute a coarse shape model of the asteroid. The Lutetia flyby case turned out to be not a very suitable for this method, due to the limited number of images, acquired under a very limited set of viewing and illumination conditions. Nevertheless, this robust method could still fit the contours of the asteroid in the images very accurately. It is expected that the observing conditions at the comet allow a much more accurate determination of the shape, and that this method will be sufficient for the needs of the S/C navigation around the comet.

5. References

[1] M. Lauer, S. Kielbassa, U. Herfort, D. Hocken, "Optical Measurements for the Flyby Navigation of Rosetta at Asteroid Steins", Proceedings 21st International Symposium on Space Flight Dynamics – 21st ISSFD. Toulouse, France, 2009.

[2] R.W.Gaskell et al., "Characterizing and navigating small bodies with imaging data", Meteoritics and Planetary Science 43, Nr. 6, 1049-1061 (2008).

[3] D. Wokes, J. Essert, "Development of Rosetta's Initial Stage Comet Rendezvous Guidance Systems", AIAA GNC/AFM/MST/ASC 2012

[4] T. Morley, "Rosetta navigation for the fly-by of asteroid 21 Lutetia", International Symposium on Space Flight Dynamics – 23rd ISSFD. Pasadena, USA, 2012

[5] T. Morley, "Rosetta - reconstruction of relative trajectory at Lutetia fly-by", ESA Lotus note, 27/07/2010

[6] B. Carry et. al., "Physical Properties of ESA/NASA Rosetta target asteroid (21) Lutetia: Shape and flyby geometry", Astronomy and Astrophysics 2010

[7] H. Sierks et. al., "Images of Asteroid 21 Lutetia: A Remnant Planetesimal From the Early Solar System", Science Volume 334, October 2011

[8] L. Jordan, "Lutetia Landmarks", email, 25/5/2011

[9] F. Scholten, "Lutetia Landmarks", email, 1/6/2011

[10] S. Savarese, H. Rushmeier, F. Bernardini, P. Perona: "Implementation of a Shadow Carving System for Shape Capture", in Proc. of 1st International Symposium on 3D Data Processing Visualization and Transmission , pp.12, 2002

[11] M. Kueppers, Lutetia shape model, email, 15/1